Russ. J. Earth. Sci., Vol. 22, ES3004
https://doi.org/10.2205/2022ES000795

Russian Journal of Earth Sciences

On some possibilities of multi-frequency remote sensing of the water surface

Yuriy A. Titchenko*[1], Vladimir Yu. Karaev[1], and Yijun He[2]

[1] *Institute of Applied Physics of the Russian Academy of Sciences (IAP RAS), Nizhny Novgorod, Russia*
[2] *School of Marine Sciences, Nanjing University of Information Science and Technology, Nanjing, China*

Received 24 February 2022; accepted 21 March 2022; published 31 May 2022.

This study is aimed at expanding the number of measured parameters to analyze the features of the formation of surface waves under the influence of wind. The paper develops an original approach to obtaining information on the variability of the short-wave part of the wave spectrum (examples are given for wavelengths from about 50 cm to 2 cm in 6 intervals) and the long-wave component of the wave spectrum (> 1 m) in marine conditions. To illustrate the approach, a six-frequency underwater acoustic wave gauge was simulated, which measures the slope variance of the large-scale waves, compared to the radiation wavelength, for each radiation frequency. The work is caried out a theoretical analysis of slope variance retrieved from reflected acoustic pulses for different radiation frequencies depending on the near-surface wind speed and swell wave height. For comparison, a study of a new parameter, the differential slope variance, is carried out, which contains information about short waves in the intervals of cut-off wavenumbers corresponding to the radiation frequencies. It is shown that the use of differential slope variances of the large-scale waves makes it possible to get clear of the influence of swell in the case of mixed waves and obtain a better correlation with the wind speed. The paper proposes a method for retrieving the exponent of the spectral slope in the intervals of cut-off wavelength corresponded to the radiation frequencies. Within this method, it is possible to retrieve the cut-off wavenumbers for each radiation frequency.

Keywords: Air/sea interactions, Instruments and techniques, Ocean observing systems, Ocean remote sensing statistically rough wave, scattering surface, antenna radiation pattern, Kirchhoff approximation, quasi-specular scattering, slope variance, height variance, significant wave height, multifrequency remote sensing, underwater acoustic wave gauge, small-scale waves, height spectrum, slope spectrum, swell.

Citation: Yuriy A. Titchenko, Vladimir Yu. Karaev, and Yijun He, (2022), On some possibilities of multi-frequency remote sensing of the water surface, *Russ. J. Earth. Sci.*, Vol. 22, ES3004, 10.2205/2022ES000795.

Introduction

The measurement of surface waves is an important task for studying the processes of interaction between the atmosphere and the ocean, which have a huge impact on the Earth's climate. Information about the small-scale part of surface waves is extremely important because it determines the exchange of momentum, heat, mass and energy between the ocean and the atmosphere. It was shown in [*Hwang and Wang*, 2004; *Hwang*, 2005; *Troitskaya and Rybushkina*, 2008] that 80% of the surface "roughness" is determined by waves less than 3 m long, therefore the small-scale part of surface waves is extremely important for solving a wide range of problems related to oceanology.

There are many wave spectrum models developed for solving different problems and covering all scales of waves on the water surface. There are both frequency spectra, for example [*Ryabkova et al.*, 2019; *Hasselmann et al.*, 1973; *Karaev et al.*, 2008] and wavenumber spectra, for example [*Elfouhaily et al.*, 1997; *Apel*, 1994; *Plant*, 2002].

To "include" short waves in the wave spectrum model, it is necessary to be able to measure them. In marine conditions, this is an extremely difficult task, since at present there are no instruments capable of simultaneously measuring the large-scale and small-scale waves of the wave spectrum due to the large dynamic range of wave elevation.

Marine buoys are actively used to validate satellite scatterometers and altimeters, for example, NDBC buoys [*NDBC*, 2009] measure waves longer than 6 m–10 m. The inability to measure shorter waves is due to the large dimensions of the buoys.

Acoustic Doppler current profilers (ADCP) are one of the most convenient instruments for field measurements [*Birch et al.*, 2004] since they can be installed on the bottom in any region of interest. However, the maximum installation depth (30 m–

*Corresponding author: yuriy@ipfran.ru

60 m) and the relatively low spatial resolution of the measured waves (waves longer than 3 m–6 m are measured) limit the applicability of these instruments.

To measure the slope variance, laser wave gauges are used, which have proven themselves well in the laboratory [*Hwang*, 1999]. However, in marine conditions, large waves significantly complicate the task from the point of view of technical implementation, and the problem has not been solved. A promising approach to measure the shape of the sea surface along a selected trajectory of laser scanning with a video recording frequency develops in *Sterlyadkin et al.* [2021].

A string wave gauge is the most wide-range device among the generally recognized and in field conditions (for example, on an oceanographic platform near the Katsiveli settlement [*Dulov et al.*, 2021; *Bondur et al.*, 2016]), the wave spectrum with wavelengths of more than 1 m–1.5 m is measured.

The slope variance of a large-scale waves, compared to the radiation wavelength according to the two-scale model [*Valenzuela*, 1978; *Bass and Fuks*, 1979], can be retrieved from the data of precipitation radars installed on the satellites of the TRMM or GPM mission [*TRMM*, 2001; *G.P.M.*, 2014], as well as from the data of the SWIM radar on the CFOSAT satellite [*Hauser et al.*, 2017]. The GPM satellite is equipped with a dual-frequency precipitation radar (DPR), which performs measurements at two frequencies (Ku- and Ka-bands) at different angles of incidence in a swath of about 240 km and a spatial resolution of about 5 km. Subsequent processing makes it possible to determine the slope variance of large-scale waves for the ranges used [*Freilich and Vanhoff*, 2003; *Tran et al.*, 2007; *Panfilova et al.*, 2018]. The SWIM radar opens the possibility of measuring a two-dimensional large-scale (for Ku-band) wave slope variance field [*Karaev et al.*, 2021] However, it remains unknown which wavelengths contribute to the measured parameters, i.e., what is the cut-off wavenumber that divides the wave spectrum into large-scale and small-scale components. To answer this question, the experiments are needed.

In this regard, the development of new instruments for the simultaneous measurement of large-scale and small-scale components of the wave spectrum is important and relevant. The information will be in demand by specialists studying the interaction of the atmosphere and the ocean, developing numerical models of wind waves.

The study of the dependence of the slope variance of large-scale waves on the wavelength of microwave radiation was carried out in *Zapevalov et al.* [2020]; *Danilytchev et al.* [2009]. In *Kuznetsova et al.* [2019]; *Panfilova et al.* [2021], approaches to the validation of the WAVEWATCH III model are discussed by comparing with the slope variance of large-scale waves measured by satellite radar. Integration of the measured L-band slope variance according to the satellite data of the CYGNSS (The Cyclone Global Navigation Satellite System) mission in the WAVEWATCH III model is carried out in *Wang et al.* [2019]

This work develops the approach proposed earlier [*Titchenko et al.*, 2021b] to the description of small-scale waves on the water surface using differential slope variances. This approach uses the ability of an underwater acoustic wave gauge to measure the slope variance [*Karaev et al.*, 2014; *Titchenko et al.*, 2019] accounting waves from the longest to a cut-off wavelength, which depends on the radiation frequency and surface waves intensity. When using a multi-frequency underwater acoustic wave gauge, the difference in slope variances measured at different frequencies will contain information about waves within the cut-off wavelengths. In this work the advantage of the differential slope variance for the case of mixed waves is demonstrate on the model data.

In previous works, the possibility of determining the exponent of the spectral slope of the high-frequency part of the frequency spectrum was shown based on measuring the differential slope variances using a six-frequency acoustic wave gauge with known cut-off wavenumbers and short waves dispersion relation. In this paper, we solve the problem of determining the exponent of the spectral slope of the short-wave part of the wavenumber spectrum without setting cut-off wavenumbers. The paper considers a method for estimating unknown cut-off wavenumbers corresponding to radiation frequencies. A distinctive feature of the new method is that the dispersion relation is not used.

Problem statement

Let us assume that a six-frequency pulsed underwater acoustic wave gauge (wavelengths 8 mm, 2.1 cm, 3 cm, 5.5 cm, 10 cm, 23 cm) with wide antenna patterns (30° half power width) for each frequency is used to analyze the short-wave part of the wave spectrum in 6 intervals. An underwater acoustic wave gauge is proposed to be installed on the bottom or on a floating underwater platform so that its antennas are directed vertically upwards on the water surface, as shown in Figure 1.

To determine the slope variance of large-scale wave for each radiation frequency, two approaches, borrowed from radar and new to hydroacoustic, can be used: the first is based on the analysis of the shape of the reflected pulse [*Brown*, 1977], and the second will use the dependence of the reflected power on the angle of incidence [*Freilich and Vanhoff*, 2003; *Panfilova et al.*, 2020].

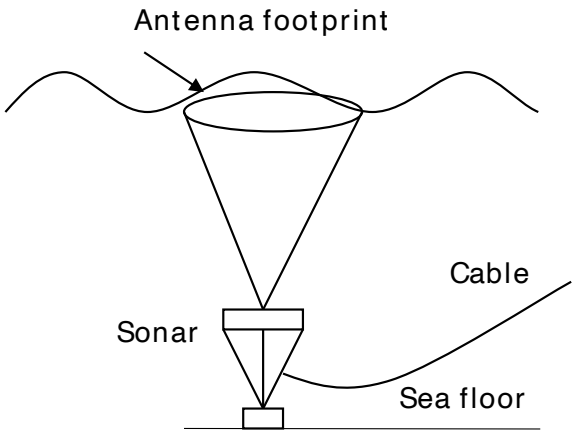

Figure 1: Measurement scheme of an underwater acoustic wave gauge.

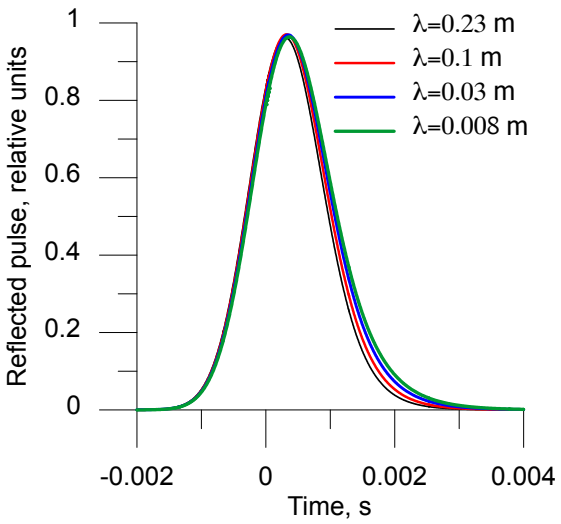

Figure 2: Reflected pulses modeled for fully developed wind waves and wind speeds of 8 m/s observed by sonars with four different wavelengths 0.008 m, 0.1 m, 0.03 m, and 0.23 m.

The first approach uses a theoretical model of a reflected pulse received by an underwater acoustic wave gauge [*Karaev et al.*, 2014]. When selecting the shape of the reflected pulse [*Titchenko et al.*, 2019], in addition to the slope variance, the water level and the significant wave height (which is four times the square roots of the wave height variance) are determined [*Titchenko et al.*, 2019].

In the framework of the second approach, the dependence of the reflected power on the angle of incidence can be measured by changing the angle of incidence. For an acoustic wave gauge with a wide antenna pattern, the method of calculating the dependence of the power of the reflected radiation on the angle of incidence without changing the orientation of the sonar antenna can be applied [*Titchenko et al.*, 2021a] i.e., the antenna remains stationary. This method is based on the geometry of the interaction of the emitted acoustic pulse with the water surface.

Figure 2 shows modeled reflected pulses for a fully developed wind wave and a wind speed of 8 m/s for four sonar wavelengths: 0.008 m, 0.1 m, 0.03 m, and 0.23 m. In the figure, the 0 s time corresponds to the duration of sound propagation from sonar to the flat surface without waves. The duration of the emitted rectangular pulse is 50 μ s. Depth 50 m. Beam width for all frequencies at half power level is 30°. The pulse amplitudes are normalized to each other to compare the slopes of the leading and trailing edges for different radiation wavelengths.

The figure shows that the difference in the duration of the leading edge of the reflected pulses received by sonar with different wavelengths is small. This is because the duration of the leading edge of the reflected pulse is determined by the wave height variances, which will be close for these wavelengths. The trailing edge is highly dependent on the sonar wavelength, as it is determined by the slope variance of large-scale waves, which depends on the radiation wavelength.

Thus, an underwater acoustic wave gauge for each radiation wavelength can measure the slope variance and the height variance of the water surface [*Titchenko et al.*, 2019].

The slope variance of large-scale waves, measured by a sonar or radar, is determined by the integral of the slope spectrum calculated in the range from 0 to the cut-off wavenumber:

$$\sigma_s^2(\lambda) = \int_0^{\kappa_c(\lambda)} \kappa^2 S(\kappa) d\kappa, \qquad (1)$$

where $S(\kappa)$ is the wavenumber spectrum; κ– wavenumber of a wave on the sea surface. The value of the cut-off wavenumber $\kappa_c(\lambda)$ depends on the wind speed and radiation wavelength [*Bass and Fuks*, 1979]. In the case of optical observations, such as in the experiment of Cox and Munk [*Cox and Munk*, 1954] the cut-off wavenumber can be considered infinite, since in this case all waves present on the surface are considered. Also, all the waves available on the sea surface can be observed by a sonar with a radiation wavelength of 2 mm. Such a slope variance with infinite cut-off wavenumber will henceforth be called optical.

Height variance is calculated by the following formula:

$$\sigma_H^2(\lambda) = \int_0^{\kappa_c(\lambda)} S(\kappa) d\kappa. \qquad (2)$$

Figure 3 shows the location of the cut-off wavenumbers corresponding to the used radiation wavelength of the underwater acoustic wave gauge

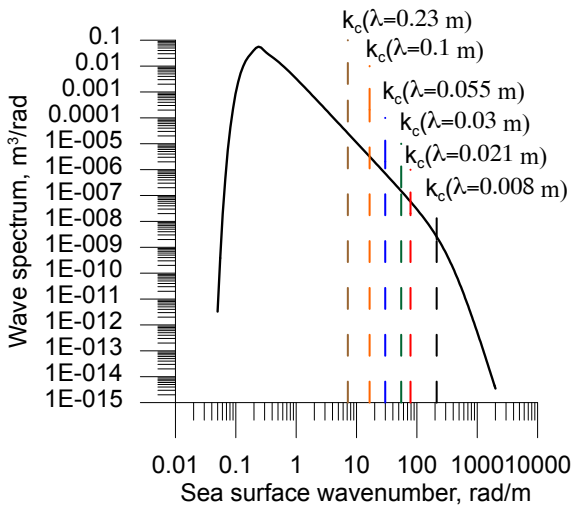

Figure 3: The location of the cut-off wavenumbers corresponding to the radiation wavelengths of the underwater acoustic wave gauge on the wavenumber spectrum model for a fully developed wind wave and a wind speed of 8 m/s.

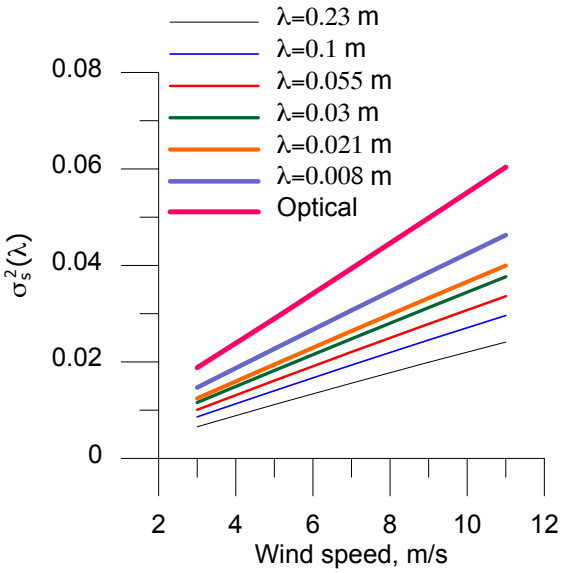

Figure 4: Slope variances of large-scale waves as a function of wind speed for different radiation wavelengths. In all cases, there is a 200 m long swell.

on the wavenumber spectrum model [*Karaev et al.*, 2008], for the case of a fully developed wind wave and a wind speed of 8 m/s.

Differences in the slope variances of large-scale waves, measured by multi-frequency acoustic wave gauge, will be determined by the integral over the slope spectrum within the cut-off wavenumbers of the analyzed radiation wavelengths:

$$\Delta\sigma_s^2(2-1) = \sigma_s^2(\lambda_2) - \sigma_s^2(\lambda_1) = \int_{\kappa_c(\lambda_1)}^{\kappa_c(\lambda_2)} \kappa^2 S(\kappa) d\kappa \quad (3)$$

Thus, this differential slope variance will contain information about the waves in the selected wavelength range. This parameter will be the object of further research.

Slope variance and differential slope variance

Let us consider the slope variance of large-scale waves retrieved from the simulated shape of the reflected pulse for different radiation wavelengths depending on the near-surface wind speed (Figure 4).

The dependences were obtained for a mixed wave formed by a fully developed wind waves and swell 200 m long with a significant swell height of 3.2 m.

It can be seen from the figure that the slope variance, which includes a larger range of surface wavelengths (radiation wavelength is shorter), is more sensitive to the wind speed.

Further, according to these slope variances, in Figure 5, the differential slope variances is constructed in 6 intervals of cut-off wavenumbers corresponding to the radiation wavelengths of a multi-frequency acoustic wave gauge. The differential slope variance is obtained by subtracting the slope variances for the corresponding radiation wavelengths from the optical slope variance.

It can be seen from the figure that the sensitivity to wind speed of the differential slope variance decreases with decreasing radiation wavelength. This confirms that the differential slope variance, which consider a larger range of surface wavelengths, are more sensitive to wind speed.

A feature of the differential slope variance is the subtraction of large-scale waves, which may include swells and other waves propagating over long distances. The wavenumber spectrum with a 200 m long swell set according to the spectrum model [*Karaev et al.*, 2008] as shown in Figure 6.

Figure 6 shows that the long-wave part of the spectrum changes significantly with the addition of swell. In this case, the short-wave part does not change when swell is added. Next, we consider the effect of swell of different heights on slope variance and differential slope variances according to Figure 7. The figure shows the relative deviation of the measured slope variance and differential slope variance from the value for purely wind waves in dependance on significant swell height as

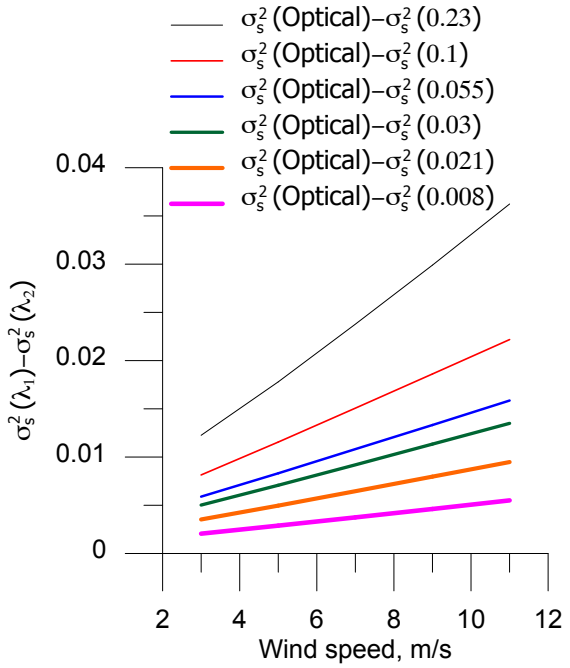

Figure 5: Differential slope variance in 6 intervals of cut-off wavenumbers corresponding to the radiation wavelengths depending on wind speed.

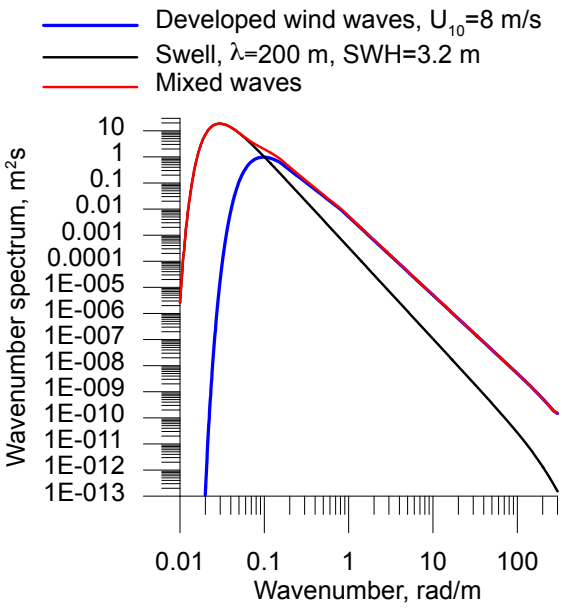

Figure 6: Spectrum of swell, wind waves and mixed waves.

a percentage of purely wind slope variance. Wind waves in all cases, fully developed at a wind speed of 8 m/s.

It can be seen from the figure that the swell has practically no effect on the differential slope variance. Thus, the differential slope variance will be determined only by the waves caused by the instantaneous wind, which makes it more stable compared to the slope variance in real measurements. Also, when analyzing the differential slope variance, the need to consider multimode waves is eliminated.

Determination of the exponent of the spectral slope

The short-wave part of the wavenumber spectrum is given at different intervals of the wavenumber in the form of various power-law functions of the wavenumber [*Plant*, 2002; *Phillips*, 1985; *Elfouhaily et al.*, 1997; *Apel*, 1994]:

$$S(\kappa) = \frac{A}{\kappa^N}, \tag{4}$$

where A is a constant for a given interval of wavenumbers, N is the exponent of the spectral slope.

The differential slope variance can be written as follows, considering (4):

$$\Delta\sigma_s^2(2-1) = \int_{\kappa_c(\lambda_1)}^{\kappa_c(\lambda_2)} \kappa^2 \frac{A}{\kappa^N} d\kappa = \frac{A}{3-N}\left({\kappa_c}^{3-N}(\lambda_2) - {\kappa_c}^{3-N}(\lambda_1)\right). \tag{5}$$

Consider that we do not know the cut-off wavenumbers, the constant A, and the exponent of the spectral slope N.

It should also be noted here that N>2, since the short-wave part of the slope spectrum, $\frac{A}{\kappa^{N-2}}$, cannot grow with an increase in the wavenumbers κ, unlike, for example, the curvature spectrum [*Elfouhaily et al.*, 1997; *Karaev et al.*, 2008].

Additionally, the following equation can be written for the difference in slope variances obtained by optics and measured by an underwater acoustic wave gauge with a radiated wavelength λ_1:

$$\Delta\sigma_s^2(optical-1) = \sigma_s^2(optical) - \sigma_s^2(\lambda_1) - \frac{A{\kappa_c}^{3-N}(\lambda_1)}{3-N}, \tag{6}$$

where $\sigma_s^2(optical)$ is the slope variance according to optical measurements, it include waves of all scales that exist on the water surface. There are works in which the optical slope variance is measured from underwater [*Molkov et al.*, 2019; *Molkov*, 2020]. Using a sonar with a wavelength

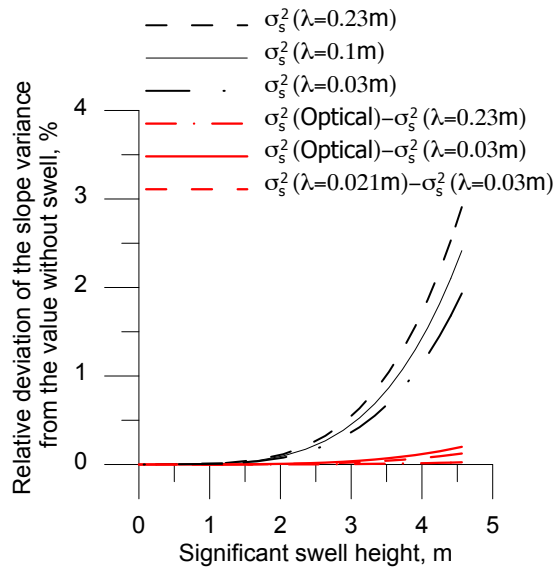

Figure 7: Relative deviation of the measured slope variance and differential slope variance from the value for pure wind waves in dependence on a significant swell height.

of 2 mm, the same slope variance will also be measured. Thus, synchronous measurement of optical slope variance can be organized from a floating or bottom platform of an underwater acoustic wave gauge.

The parameter $\Delta\sigma_s^2(optical-1)$ is determined by all small-scale waves from the cut-off wavenumbers $\kappa_c(\lambda_1)$ to infinity.

Also, to retrieve all the parameters, we need such a parameter as the differential height variance:

$$\Delta\sigma_H^2(2-1) = \int_{\kappa_c(\lambda_1)}^{\kappa_c(\lambda_2)} \frac{A}{\kappa^N} d\kappa = \frac{A}{1-N}\left(\kappa_c^{1-N}(\lambda_2) - \kappa_c^{1-N}(\lambda_1)\right). \tag{7}$$

This parameter can be obtained by measuring the height variance for each radiation wavelength from the shape of the reflected pulse [*Karaev et al.*, 2014; *Titchenko et al.*, 2019; *Ryabkova et al.*, 2021] using a multi-frequency acoustic wave gauge. It should be noted here that this parameter cannot be measured for any combination of sonar wavelengths. The point is that the height variance is determined mainly by long waves, and as the wavelength decreases, their contribution to the height variance rapidly weakens. This can be seen even from formulas where the exponent in (7) is less than in (6) by 2.

As a result, having a three-frequency underwater acoustic wave gauge and measuring three slope variances, three height variances and knowing (measuring) the optical slopes, we obtain the following system of equations:

$$\begin{aligned}
\Delta\sigma_s^2(2-1) &= \frac{A}{3-N}\left(\kappa_c{}^{3-N}(\lambda_2) - \kappa_c{}^{3-N}(\lambda_1)\right),\\
\Delta\sigma_s^2(3-1) &= \frac{A}{3-N}\left(\kappa_c{}^{3-N}(\lambda_3) - \kappa_c{}^{3-N}(\lambda_1)\right),\\
\Delta\sigma_s^2(optical-1) &= -\frac{A\kappa_c{}^{3-N}(\lambda_1)}{3-N},\\
\Delta\sigma_H^2(2-1) &= \frac{A}{1-N}\left(\kappa_c^{1-N}(\lambda_2) - \kappa_c^{1-N}(\lambda_1)\right),\\
\Delta\sigma_H^2(3-1) &= \frac{A}{1-N}\left(\kappa_c^{1-N}(\lambda_3) - \kappa_c^{1-N}(\lambda_1)\right).
\end{aligned} \tag{8}$$

The system contains 5 unknowns and 5 equations.

After simple transformations, we obtain the following expression containing only one unknown:

$$\frac{\Delta\sigma_H^2(2-1)}{\Delta\sigma_H^2(3-1)}\left(\left(1-\frac{\Delta\sigma_s^2(3-1)}{\Delta\sigma_s^2(optical-1)}\right)^{\frac{1-N}{3-N}}-1\right) = \left(1-\frac{\Delta\sigma_s^2(2-1)}{\Delta\sigma_s^2(optical-1)}\right)^{\frac{1-N}{3-N}}-1. \tag{9}$$

Minimizing the difference between the left and right parts, we numerically find the exponent of the spectral slope N. Then, knowing N, we consequently express the remaining unknowns:

$$\begin{aligned}
k_1 &= \sqrt{\frac{3-N}{1-N}\Delta\sigma_s^2(C\&M-1)\frac{1-\left(1-\frac{\Delta\sigma_s^2(3-1)}{\Delta\sigma_s^2(C\&M-1)}\right)^{\frac{1-N}{3-N}}}{\Delta\sigma_H^2(3-1)}},\\
k_3 &= k_1\left(1-\frac{\Delta\sigma_s^2(3-1)}{\Delta\sigma_s^2(C\&M-1)}\right)^{\frac{1}{3-N}},\\
k_2 &= k_1\left(1-\frac{\Delta\sigma_s^2(2-1)}{\Delta\sigma_s^2(C\&M-1)}\right)^{\frac{1}{3-N}},\\
A &= \frac{\Delta\sigma_s^2(2-1)(3-N)}{k_2{}^{3-N}-k_1{}^{3-N}}.
\end{aligned} \tag{10}$$

Let us check the above algorithm using the spectrum model [*Karaev et al.*, 2008]. To do this, using the spectrum model, we calculate the slope and height variances of large-scale waves for five wavelengths, 0.23 m, 0.1 m, 0.055 m, 0.03 m, 0.021 m for wind speeds from 3 m/s to 11 m/s with fully developed wind waves. We calculate optical slope variance integrating full spectrum model. Next, for two combinations of wavelengths, we will retrieve all unknown parameters in dependance on wind speed, which are shown on the left and right plots in Figure 8.

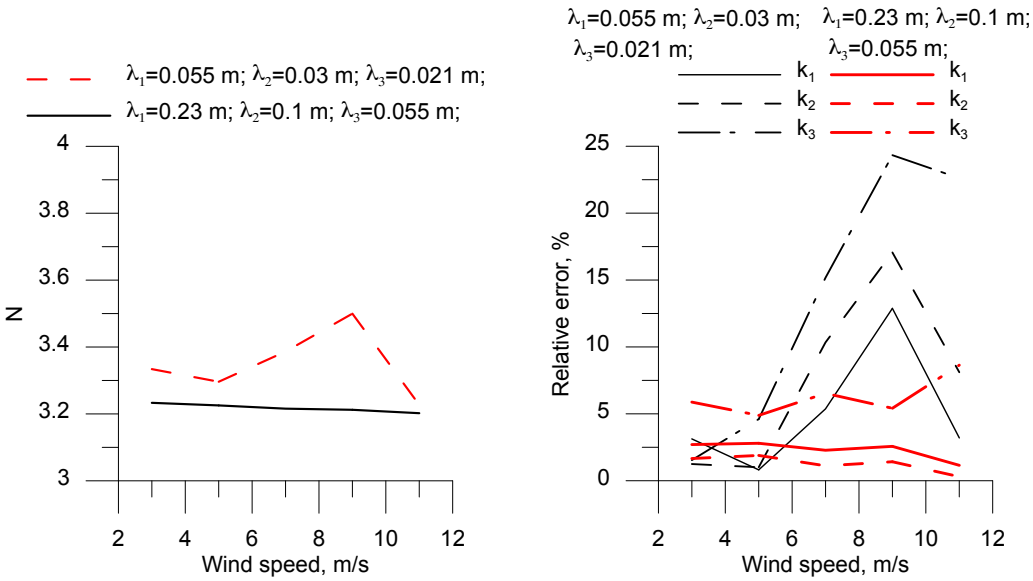

Figure 8: Retrieved from model measurements, the exponent of the spectral slope N (left) and the relative error of retrieving the cut-off wavenumbers depending on wind speed for two combinations of wavelengths of a three-frequency acoustic wave gauges

The left plot in Figure 8 shows that the shorter-wave part of the spectrum falls off more strongly than the longer-wave one, which corresponds to the assumption of a faster decrease in the amplitude of shorter waves.

The right plot in Figure 8 shows that for the longer-wave "triple" of radiation wavelengths, the error in determining the exponent of the spectral slope is usually smaller and the result is more stable. Since the height variances are determined mainly by long waves (large-scale waves), and the short-wave part of the spectrum (small-scale waves) makes a small contribution, it is therefore desirable to use the maximum radiation wavelengths separation to obtain a greater difference in height variance, which will increase the accuracy of the proposed algorithm (10).

Let us illustrate the operation of algorithm (10) in comparison with the spectrum model [*Karaev et al.*, 2008] used to calculate the wave parameters in Figure 9. The calculations will be carried out for a fully developed wind waves and a wind speed of 3 m/s.

The retrieved wavenumber spectra are shown within the limits of the wavenumbers obtained as a result of calculation by formulas (10). The figure shows a satisfactory agreement between the retrieved spectra and the spectrum model used to calculate the wave parameters required for algorithm (10). Some difference between the curves on the plot is due to the error in calculating the differential height variance (7).

In previous work [*Titchenko et al.*, 2021b], the selected exponent of the spectral slope in the high-

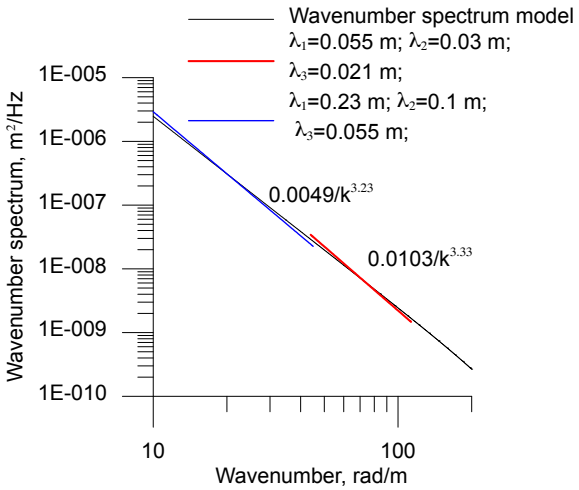

Figure 9: Wavenumber spectra retrieved from model measurements for two combinations of radiation wavelengths of a three-frequency acoustic wave gauge in comparison with the wavenumber spectrum model

frequency part of the frequency spectrum was obtained approximately equal to 5 for a fully developed wave and a wind speed of 3 m/s, which corresponds to the spectrum model used [*Karaev et al.*, 2008]. For the wavenumber spectrum, this corresponds (using dispersion relation for gravity-capillary waves) approximately to the exponent of the spectral slope of 3.4 for longer waves and 3.2 for shorter ones. This matches the obtained result in Figure 9.

It is important to note that the proposed algorithm will be ineffective in marine conditions when radiation wavelengths shorter than 3 cm are chosen due to the differential height variance used, since the spectrum in this range has extremely small values. The efficiency of the proposed method will increase with the growth of the "scatter" of radiation wavelengths, i.e., when the differential height variance increases.

Conclusions

In this work, a theoretical study of new possibilities of multi-frequency remote sensing has been carried out. For measurements, it is proposed to use a multi-frequency underwater acoustic wave gauge. The multi-frequency system measures the slope variance in different wavelength intervals, which makes it possible to separate the contribution of the large-scale and small-scale components of the wave spectrum to the slope variance. The paper proposes to use the differential slope variance to describe the short-wave part of the wave spectrum. It is shown that the use of differential slope variances of the large-scale waves makes it possible to get clear of the influence of swell in the case of mixed waves and obtain a better correlation with the wind speed.

An original algorithm for retrieving the short-wave part of the wavenumber spectrum, as well as cut-off wavenumbers of radiation wavelengths, has been developed. Moreover, to determine the wave spectrum and cut-off wavenumbers, it is not required to set the dispersion relation for short waves. It is noted that for the best operation of the algorithm in real conditions, it is necessary to use an underwater acoustic wave gauge with a larger difference in the radiation wavelengths.

This new information about waves will allow studying the interaction of wind simultaneously with the short-wave and long-wave components of the wavenumber spectrum and will be in demand by scientists involved in numerical simulation modeling of the wave climate and interested in refining the model of near-surface wind-wave interaction. In addition, new information about the short-wave part of the elevation spectrum in different wavelength ranges will improve the accuracy of near-surface wind speed retrieval from remote sensing data.

Acknowledgments

The study was carried out at the expense of a grant from the Russian Science Foundation (project No. 20-77-10089).

References

Apel, J. R., An improved model of the ocean surface wave vector spectrum and its effects on radar backscatter, *Journal of Geophysical Research: Oceans*, *99*(C8), 16,269–16,291, doi:10.1029/94JC00846, 1994.

Bass, F., and I. Fuks, Preface to the russian edition, in *Wave Scattering from Statistically Rough Surfaces*, *International Series in Natural Philosophy*, vol. 93, edited by F. Bass and I. Fuks, pp. ix–x, Pergamon, doi:10.1016/B978-0-08-019896-5.50004-2, 1979.

Birch, R., D. Fissel, K. Borg, V. Lee, and D. English, The capabilities of doppler current profilers for directional wave measurements in coastal and nearshore waters, in *Oceans '04 MTS/IEEE Techno-Ocean '04 (IEEE Cat. No.04CH37600)*, vol. 3, pp. 1418–1427 Vol.3, doi:10.1109/OCEANS.2004.1406330, 2004.

Bondur, V. G., V. A. Dulov, A. B. Murynin, and Y. Y. Yurovsky, A study of sea-wave spectra in a wide wavelength range from satellite and in-situ data, *Izvestiya, Atmospheric and Oceanic Physics*, *52*(9), 888–903, doi:10.1134/S0001433816090097, 2016.

Brown, G., The average impulse response of a rough surface and its applications, *IEEE Transactions on Antennas and Propagation*, *25*(1), 67–74, doi:10.1109/TAP.1977.1141536, 1977.

Cox, C., and W. Munk, Measurement of the roughness of the sea surface from photographs of the sun's glitter, *J. Opt. Soc. Am.*, *44*(11), 838–850, doi:10.1364/JOSA.44.000838, 1954.

Danilytchev, M. V., B. G. Kutuza, and A. G. Nikolaev, The application of sea wave slope distribution empirical dependences in estimation of interaction between microwave radiation and rough sea surface, *IEEE Transactions on Geoscience and Remote Sensing*, *47*(2), 652–661, doi:10.1109/TGRS.2008.2004410, 2009.

Dulov, V. A., A. E. Korinenko, V. N. Kudryavtsev, and V. V. Malinovsky, Modulation of wind-wave breaking by long surface waves, *Remote Sensing*, *13*(14), doi:10.3390/rs13142825, 2021.

Elfouhaily, T., B. Chapron, K. Katsaros, and D. Vandemark, A unified directional spectrum for long and short wind-driven waves, *Journal of Geophysical Research: Oceans*, *102*(C7), 15,781–15,796, doi:10.1029/97JC00467, 1997.

Freilich, M. H., and B. A. Vanhoff, The relationship between winds, surface roughness, and radar backscatter at low incidence angles from trmm precipitation radar measurements, *Journal of Atmospheric and Oceanic Technology*, *20*(4), 549–562, doi:10/cvgw86, 2003.

G.P.M., *GPM Data Utilization Handbook*, Tokyo, 1s ed., 2014.

Hasselmann, K., T. P. Barnett, E. Bouws, H. Carlson, D. E. Cartwright, K. Enke, J. A. Ewing, A. Gienapp, D. E. Hasselmann, P. Kruseman, et al., Measurements of wind-wave growth and swell decay during the Joint North Sea Wave Project (JONSWAP), *Ergaenzungsheft zur Deutschen Hydrographischen Zeitschrift, Reihe A, A8*, 1–95, 1973.

Hauser, D., C. Tison, T. Amiot, L. Delaye, N. Corcoral, and P. Castillan, SWIM: The First Spaceborne Wave Scatterometer, *IEEE Transactions on Geoscience and Remote Sensing*, *55*(5), 3000–3014, doi:10.1109/TGRS.2017.2658672, 2017.

Hwang, P., Microstructure of Ocean Surface Roughness: A Study of Spatial Measurement and Laboratory Investigation of Modulation Analysis, *Journal of Atmospheric and Oceanic Technology*, *16*(11), 1619–1629, doi:10/dtgs5j, 1999.

Hwang, P. A., Wave number spectrum and mean square slope of intermediate-scale ocean surface waves, *Journal of Geophysical Research: Oceans*, *110*(C10), doi:10.1029/2005JC003002, 2005.

Hwang, P. A., and D. W. Wang, An empirical investigation of source term balance of small scale surface waves, *Geophysical Research Letters*, *31*(15), doi:https://doi.org/10.1029/2004GL020080, 2004.

Karaev, V., M. Kanevsky, and E. Meshkov, The effect of sea surface slicks on the doppler spectrum width of a backscattered microwave signal, *Sensors*, *8*(6), 3780–3801, doi:10.3390/s8063780, 2008.

Karaev, V., M. Panfilova, M. Ryabkova, Y. Titchenko, E. Meshkov, and X. Li, Retrieval of the two-dimensional slope field by the SWIM spectrometer of the CFOSAT satellite: Discussion of the algorithm, *Russian Journal of Earth Sciences*, *21*(6), 1–9, doi:10.2205/2021es000784, 2021.

Karaev, V. Y., M. E. Meshkov, and Y. L. Titchenko, Underwater Acoustic Altimeter, *Radiophysics and Quantum Electronics*, *57*(7), 488–497, doi:10.1007/s11141-014-9531-8, 2014.

Kuznetsova, A., M. Panfilova, Y. Titchenko, G. Baydakov, and Y. Troitskaya, Study of waves at different fetches using WAVEWATCH III modeling and precipitation radar data, in *OCEANS 2019 - Marseille*, pp. 1–5, doi:10.1109/OCEANSE.2019.8867107, 2019.

Molkov, A. A., Retrieval of slope spectrum of sea roughness by Snell's window imagery: theory and numerical experiment (one-dimensional sea roughness), in *Remote Sensing of the Ocean, Sea Ice, Coastal Waters, and Large Water Regions 2020*, vol. 11529, edited by C. R. B. Jr., X. Neyt, and F. Viallefont-Robinet, pp. 61–68, International Society for Optics and Photonics, SPIE, doi:10.1117/12.2573949, 2020.

Molkov, A. A., L. S. Dolin, I. A. Kapustin, and O. V. Shomina, The retrieval of wind wave characteristics by the underwater solar path image: slope frequency spectrum, in *Remote Sensing of the Ocean, Sea Ice, Coastal Waters, and Large Water Regions 2019*, vol. 11150, edited by C. R. B. Jr., X. Neyt, and F. Viallefont-Robinet, pp. 328–331, International Society for Optics and Photonics, SPIE, doi:10.1117/12.2533010, 2019.

NDBC, *Handbook of Automated Data Quality Control Checks and Procedures*, 2009.

Panfilova, M., V. Karaev, and J. Guo, Oil slick observation at low incidence angles in ku-band, *Journal of Geophysical Research: Oceans*, *123*(3), 1924–1936, doi:10.1002/2017JC013377, 2018.

Panfilova, M., V. Karaev, L. Mitnik, Y. Titchenko, M. Ryabkova, and E. Meshkov, Advanced View at the Ocean Surface, *Journal of Geophysical Research: Oceans*, *125*(11), 2020 016,531, doi:10.1029/2020JC016531, 2020.

Panfilova, M., A. M. Kuznetsova, Y. A. Titchenko, D. A. Sergeev, Y. I. Troitskaya, and V. Y. Karaev, Methods of comparing the wave model simulation data with the ka-band radar data, in *2021 IEEE International Geoscience and Remote Sensing Symposium IGARSS*, pp. 7537–7540, doi:10.1109/IGARSS47720.2021.9555041, 2021.

Phillips, O. M., Spectral and statistical properties of the equilibrium range in wind-generated gravity waves, *Journal of Fluid Mechanics*, *156*, 505–531, doi:10.1017/S0022112085002221, 1985.

Plant, W. J., A stochastic, multiscale model of microwave backscatter from the ocean, *Journal of Geophysical Research: Oceans*, *107*(C9), 3–1–3–21, doi:10.1029/2001JC000909, 2002.

Ryabkova, M., V. Karaev, J. Guo, and Y. Titchenko, A review of wave spectrum models as applied to the problem of radar probing of the sea surface, *Journal of Geophysical Research: Oceans*, *124*(10), 7104–7134, doi:https://doi.org/10.1029/2018JC014804, 2019.

Ryabkova, M., V. Titov, Y. Titchenko, E. Meshkov, V. Karaev, A. Yablokov, K. Ponur, R. Belyaev, and M. Panfilova, Measurements of the sea surface waves parameters and the doppler spectrum of the reflected signal using optical and acoustic remote sensing methods, in *2021 XXXIVth General Assembly and Scientific Symposium of the International Union of Radio Science (URSI GASS)*, pp. 1–4, doi:10.23919/URSIGASS51995.2021.9560283, 2021.

Sterlyadkin, V. V., K. V. Kulikovsky, A. V. Kuzmin, E. A. Sharkov, and M. V. Likhacheva, Scanning laser wave recorder with registration of "instantaneous" sea surface profiles, *Journal of Atmospheric and Oceanic Technology*, *38*(8), 1415 – 1424, doi:10.1175/JTECH-D-21-0036.1, 2021.

Titchenko, Y., V. Karaev, M. Ryabkova, A. Kuznetsova, and E. Meshkov, Peculiarities of the Acoustic Pulse Formation Reflected by the Water Surface: a Numerical Experiments and the Results of Long-term Measurements Using the "Kalmar" Sonar, in *OCEANS 2019 - Marseille*, pp. 1–7, doi:10.1109/OCEANSE.2019.8867467, 2019.

Titchenko, Y., V. Karaev, M. Ryabkova, K. Ponur, E. Meshkov, and R. Belyaev, Backscattering cross-section incident dependence by reflected pulse shape using a fixed antenna with the wide antenna pattern, in *2021 IEEE International Geoscience and Remote Sensing Symposium IGARSS*, pp. 7398–7401, doi:10.1109/IGARSS47720.2021.9553689, 2021a.

Titchenko, Y. A., V. Y. Karaev, M. S. Ryabkova, E. M. Meshkov, K. A. Ponur, and R. V. Belyaev, Theoretical view on the possibilities of multi-frequency remote sensing of the water surface, in *2021 Photonics Electromagnetics Research Symposium (PIERS)*, pp. 2370–2376, doi:10.1109/PIERS53385.2021.9694705, 2021b.

Tran, N., B. Chapron, and D. Vandemark, Effect of long waves on ku-band ocean radar backscatter at low incidence angles using trmm and altimeter data, *IEEE Geoscience and Remote Sensing Letters*, *4*(4), 542–546, doi:10.1109/LGRS.2007.896329, 2007.

TRMM, *TRMM Data Users Handbook*, Tokyo, 2001.

Troitskaya, Y. I., and G. V. Rybushkina, Quasi-linear model of interaction of surface waves with strong and hurricane winds, *Izvestiya, Atmospheric and Oceanic Physics*, *44*(5), 621–645, doi:10.1134/S0001433808050083, 2008.

Valenzuela, G. R., Theories for the interaction of electromagnetic and oceanic waves —a review, *Boundary-Layer Meteorology*, *13*(1), 61–85, doi:10.1007/BF00913863, 1978.

Wang, T., V. U. Zavorotny, J. Johnson, Y. Yi, and C. Ruf, Integration of Cygnss Wind and Wave Observations with the Wavewatch III Numerical Model, in *IGARSS 2019 – 2019 IEEE International Geoscience and Remote Sensing Symposium*, pp. 8350–8353, doi:10.1109/IGARSS.2019.8900481, 2019.

Zapevalov, A. S., I. P. Shumeyko, and A. Y. Abramovich, Dependences of the characteristics of sea surface slopes on the spatial ranges of the waves creating them, *Zhurnal Radioelektroniki*, *2020*(5), doi:10.30898/1684-1719.2020.5.15, (in Russian), 2020.